Cellular Physiology and Biochemistry

Cell Physiol Biochem 2018;48:2563-2582
DOI: 10.1159/000492700
Published online: 16 August, 2018
Accepted: 7 August, 2018

Original Paper

Tuning of Differential Lipid Order Between Submicrometric Domains and Surrounding Membrane Upon Erythrocyte Reshaping

Catherine Leonard[a,b] Hélène Pollet[b] Christiane Vermylen[c] Nir Gov[d] Donatienne Tyteca[b] Marie-Paule Mingeot-Leclercq[a]

[a]FACM Unit, Louvain Drug Research Institute & Université Catholique de Louvain, Brussels, [b]CELL Unit, de Duve Institute & Université Catholique de Louvain, Brussels, [c]PEDI Unit, Institut de Recherche Expérimentale et Clinique & Université Catholique de Louvain, Brussels, Belgium, [d]Department of Chemical and Biological Physics, Weizmann Institute of Science, Rehovot, Israel

Key Words
Membrane lateral heterogeneity • Laurdan • Red blood cell aging • Cell deformation • Membrane vesiculation • His-mCherry-Theta-D4 • His-mCherry-NT-Lysenin • Membrane curvature • Cytoskeleton • Vital confocal imaging • Sphingomyelin • Cholesterol • Calcium exchanges

Abstract
Background/Aims: Transient nanometric cholesterol- and sphingolipid-enriched domains, called rafts, are characterized by higher lipid order as compared to surrounding lipids. Here, we asked whether the seminal concept of highly ordered rafts could be refined with the presence of lipid domains exhibiting different enrichment in cholesterol and sphingomyelin and association with erythrocyte curvature areas. We also investigated how differences in lipid order between domains and surrounding membrane (bulk) are regulated and whether changes in order differences could participate to erythrocyte deformation and vesiculation. ***Methods:*** We used the fluorescent hydration- and membrane packing-sensitive probe Laurdan to determine by imaging mode the Generalized Polarization (GP) values of lipid domains *vs* the surrounding membrane. ***Results:*** Laurdan revealed the majority of sphingomyelin-enriched domains associated to low erythrocyte curvature areas and part of the cholesterol-enriched domains associated with high curvature. Both lipid domains were less ordered than the surrounding lipids in erythrocytes at resting state. Upon erythrocyte deformation (elliptocytes and stimulation of calcium exchanges) or membrane vesiculation (storage at 4°C), lipid domains became more ordered than the bulk. Upon aging and in membrane fragility diseases (spherocytosis), an increase in the difference of lipid order between domains and

D. Tyteca and M.-P. Mingeot-Leclercq contributed equally to this work.

Marie-Paule Mingeot-Leclercq
FACM Unit, Louvain Drug Research Institute & Université catholique de Louvain
UCL Avenue Mounier 73/B1.73.05, 1200 Brussels (Belgium)
Tel. +32 2 764 73 74; E-Mail marie-paule.mingeot@uclouvain.be

the surrounding lipids contributed to the initiation of domain vesiculation. ***Conclusion:*** The critical role of domain-bulk differential lipid order modulation for erythrocyte reshaping is discussed in relation with the pressure exerted by the cytoskeleton on the membrane.

Introduction

The differential lipid order between lipid domains and the surrounding bulk membrane is thought to be highly relevant for cell physiology [1, 2]. Accordingly, a recent study highlighted that lipid order differences arising from domain formation participate in selective sorting of membrane proteins [3]. This concept was first suggested in the 90's by the lipid raft hypothesis, which proposed that sterols and sphingolipids (SLs), due to their favorable interactions, can self-aggregate into rafts of higher lipid order as compared to the surrounding lipids (bulk), thereby mediating protein sorting and cellular functions. During the past years, evidences for such lipid membrane lateral heterogeneities have been provided in membrane and cell models of increasing complexity. First, sterol-containing biomimetic model membranes, including planar supported lipid layers and giant unilamellar vesicles (GUVs), expose the coexistence of two liquid phases, one enriched in cholesterol (Chol) and SLs of high lipid order (L_o, "raft-like") and one enriched in unsaturated lipids of low lipid order (L_d, non "raft-like") [4, 5]. Second, giant plasma membrane vesicles (GPMVs) derived from living cells [6] reveal that L_o and L_d phases in natural plasma membranes (PM) can assume a wide range of lipid order states resulting from lipid order tuning upon active cellular processes [7]. Third, cellular PMs exhibit regions of higher lipid order than the bulk lipids, either as small domains or larger areas depending on cellular processes [2, 8-10]. As an additional level of complexity, several studies on cells reveal the existence of lipid domains with a wider diversity of lipid composition, such as only partial sterol and SL co-enrichment [11-15]. Hence, segregation mechanisms distinct from favorable sterol-SL interactions are proposed, such as charge-mediated sequestration [16], integral membrane proteins [17] or membrane:cytoskeleton anchorage [18-24].

Here, we investigated on red blood cells (RBCs) (i) whether lipid domains also exhibit a lipid order which is different from the bulk; and (ii) whether and how the differential lipid order can be modulated by, and/or participate in, cellular function. The choice of RBCs to explore these questions is based on four main features. First, the RBC is the simplest human cell, with a PM linked to an underlying cytoskeleton as the only structural components, reducing interference of intracellular membranes. Second, the RBC exhibits optically-resolved lipid domains, revealed by confocal imaging upon PM trace insertion of BODIPY-lipid analogs or upon decoration of endogenous Chol and sphingomyelin (SM) by mCherry-Toxin fragments (Theta and Lysenin, respectively) [15, 25-30]. At least two types of lipid domains have been shown to coexist at the RBC PM, exhibiting differential lipid enrichment and topography: one mainly enriched in Chol (hereafter referred as Chol-enriched domains) and mostly present at the highly curved edges of the RBC biconcave membrane *vs* another co-enriched in SM and Chol (hereafter referred as SM/Chol-enriched domains) and restricted to the membrane center of lower curvature [24, 31]. Third, Chol- and SM/Chol-enriched domains are differently involved in RBC function-associated reshaping such as deformation and vesiculation [31]. *In vivo*, RBC deformation is required when it passes through the microvasculature to deliver oxygen to the tissues and is further tested for quality control when it squeezes through the narrow pores of spleen sinusoids. At the end of its 120-day lifetime, RBC deformability is lost by membrane vesiculation and is followed by RBC splenic entrapment and removal from blood circulation [32]. By using abnormally-shaped elliptocytes and by stretching healthy RBCs, we revealed that Chol-enriched domains gather in increased curvature areas of the RBC membrane edges upon deformation [31]. In contrast, SM/Chol-enriched domain abundance increases in the central membrane area in relation with secondary calcium (Ca^{2+}) efflux, a process involved in the subsequent shape and volume restoration [31]. Additionally, by mimicking RBC membrane vesiculation upon aging by storage at 4°C, we showed that

both lipid domains represent specific sites for membrane vesiculation upon aging [31]. Fourth, we recently showed by high spatial resolution atomic force microscopy that the RBC membrane is composed of lipid domains exhibiting differential local mechanical properties, which could depend on their differential association to the cytoskeleton and on their specific lipid composition [33]. However, atomic force microscopy does not allow to determine the lipid composition of the domains nor to evaluate how their mechanical properties are modulated upon RBC deformation.

We therefore used an alternative approach to investigate whether the varied lipid domains evidenced at the living RBC surface could exhibit a different lipid order than the bulk, and whether these differences could be modulated by and/or participate in RBC reshaping. To this end, RBCs were labelled with Laurdan, a membrane fluorescent dye sensitive to lipid hydration and order [34-36], and were examined at their resting state and upon *in vitro* reshaping, *i.e.* deformation and vesiculation [31]. In resting RBCs, Laurdan imaging allowed to detect the majority of SM/Chol-enriched domains associated to low erythrocyte curvature areas, part of the Chol-enriched domains associated with high curvature and a third domain population not enriched in these lipids. These various lipid domain populations exhibited a diversity of lipid order states but were all less ordered than the bulk membrane. Upon RBC deformation (elliptocytes and stimulation of Ca^{2+} exchanges) or membrane vesiculation (storage at 4°C), domains became more ordered than the bulk. In aging RBCs and in membrane fragility diseases (spherocytosis), an increase in bulk-domain lipid order difference was associated to the initiation of domain vesiculation. Altogether, differences in lipid domain order in RBC membranes are modulated upon RBC reshaping and contributed to vesiculation upon aging, suggesting their biological relevance.

Materials and Methods

Red blood cell isolation and washing

This study was approved by the Medical Ethics Institutional Committee of the Université catholique de Louvain and experiments were performed according to relevant guidelines. RBCs were freshly isolated from four healthy volunteers, one splenectomized patient with spherocytosis and one patient with hereditary elliptocytosis; each donor gave written informed consent. Blood was collected by venopuncture into dry K^+/EDTA-coated tubes and, prior experiments, diluted at 1:10 in Dulbecco's Modified Eagle Medium (DMEM containing 25 mM glucose, 25 mM HEPES and no phenol red, Invitrogen) and then washed twice by centrifugation (133 *g* for 2 min) and resuspension, as previously described [15, 25, 27-29, 31]. Incubation with pharmacological agents, labelling and confocal microscopy (see below) were performed at a dilution of 2 * 10^7 RBCs/ml in DMEM. All experiments were carried out on fresh RBCs, except for aging experiments for which RBCs were maintained at 4 °C during 1 to 15 days into the K^+/EDTA-coated tubes.

SM and Chol depletion

Modulation of PM SM and Chol contents were performed as previously described [15, 25, 31]. Briefly, washed and diluted RBCs were preincubated at room temperature (RT) in suspension under continuous agitation with 2 mU/ml *Bacillus cereus* sphingomyelinase (SMase; Sigma-Aldrich) for 10 min or with 0.25 mM methyl-ß cyclodextrin (mβCD; Sigma-Aldrich) for 30 min, all in DMEM containing 1 mg/ml bovine serum albumin (BSA; Sigma-Aldrich). All RBCs were then pelleted at 133 g for 2 min, resuspended in DMEM and analyzed by vital imaging for lipid domains (see below).

Intracellular calcium depletion

Decrease of $[Ca^{2+}]_i$ was performed as described in [31]. Briefly, washed and diluted RBCs were preincubated at RT in suspension under continuous agitation in Ca^{2+}-free homemade medium containing 1 mM Ca^{2+}-chelating agent ethylene glycol-bis(β-aminoethyl ether)-N,N,N',N'-tetraacetic acid (EGTA, Sigma-Aldrich) for 10 min, then analyzed by vital imaging for lipid domains (see below).

*Living RBC labelling with Laurdan and/or Toxins**

A stock solution of Laurdan was prepared in DMSO and conserved as described in [35]. After production, Lysenin* and Theta* were maintained at -80°C in in 20 mM NaCl supplemented with 25 mM HEPES (pH 7.2) and 5 % glycerol. Both types of probes were extemporaneously diluted in DMEM containing 1 mg/ml BSA (DMEM/BSA). Washed and diluted RBCs were labeled at RT in suspension under continuous agitation with: (i) 2.5 µM Laurdan for 60 min; or (ii) 1.25 µM Lysenin* or 0.55 µM Theta* for 25 min, as previously described [15, 25, 31]. Labelled RBCs were then pelleted at 133 *g* for 2 min and resuspended in DMEM. For RBC double-labeling with Laurdan and Toxins*, RBCs were first labeled with 2.5 µM Laurdan for 40 min, then pelleted at 133 *g* for 2 min and resuspended with 2.5 µM Laurdan and either 1.25 µM Lysenin* or 0.55 µM Theta* for 25 min, then pelleted at 133 *g* for 2 min and resuspended in DMEM.

RBC immobilization and vital confocal/multiphoton imaging

After labeling in suspension, RBCs were either spread or maintained in suspension as previously described [15, 25, 31]. Briefly, for spread RBCs, coverslips were first coated with poly-L-lysine (PLL, 70–150 kDa; Sigma-Aldrich) by incubation with PLL:DMEM (1:1, *v:v*) at 37 °C for 40 min, then washed with DMEM. PLL-coated coverslips were then incubated with labelled RBCs at 20 °C for exactly 4 min. Suspension was then removed and replaced by DMEM and attached RBCs were allowed to spread for another 4 min. The coverslip was finally placed upside down on a Lab-Tek chamber filled with DMEM and observed. For suspended RBCs, labelled RBCs were dropped to settle down in µ-Slide VI0.4 uncoated IBIDI chambers (IBIDI, Proxylab; 100 µl by channel). All preparations were examined at 20°C (except when otherwise stated) with a Zeiss LSM510 confocal/multiphoton microscope using a plan-Apochromat 63X NA 1.4 oil immersion objective, and a Nomarski prism to avoid the photoselection effect. Toxin*-labelled RBCs were imaged as previously in confocal mode [15, 25, 31], while Laurdan-labelled RBCs were visualized separately at 440 nm and 490 nm in multiphoton mode. Laurdan and Toxin*-colabelled RBCs were visualized first in the multiphoton mode for the Laurdan, then in the confocal mode for the Toxin*.

Determination of RBC area and circularity and domain topography and abundance

RBC total projected area (referred to as hemi-RBC) and circularity as well as abundance and topography of Laurdan- and Chol-enriched domains were determined on high-resolution confocal images (or transmission images when no continuous membrane labeling was observed for the bulk). Domain abundance and topography were assessed by manual counting. Total RBC projected area and RBC membrane circularity were measured from ROI selections of the membrane with the analyzed particles plugging. Membrane ROI selections were obtained by thresholding fluorescent images using default methods in Image J followed by binarisation, then RBC membrane projected contours were detected using analyzed particles plugging. When no detection was possible, domain and bulk projected contours were drawn manually on fluorescent images. These selections were then used for all the following analyses.

Determination of lipid order

Domain and membrane ROIs were obtained from the two fluorescent channels (440 and 490 nm) of Laurdan images. Domain ROI selections were determined as for the membrane (see above) but detected using analyzed particles plugging with distinct size and circularity features than for the membrane. To separate the Laurdan signal associated to the domains and the bulk, domains and bulk masks were used. Domain masks were obtained from domain ROI while bulk masks were deduced using membrane ROI subtracted from domain ROI. From these masks, three types of quantification were performed on the domains and the bulk independently. First, the two-dimensional (2D) GP map, where GP for each pixel was calculated from a ratio of the two fluorescence channels, was created using MATLAB (The MathWorks, Natick, MA). Briefly, each image was binned (2 × 2) and thresholded, then the GP image was calculated for each pixel using the GP equation as described in [35] and the G_{fact} was measured as recommended in [35]. The GP of the domains and bulk membrane were calculated by averaging pixels from a large representative area (35 RBCs). The determination of domains localized or not with the Toxins*, and the following separation of the domain masks, was done manually by comparing Laurdan and Theta* images. Second, the two domain populations exposing different lipid order (P1 and P2) were studied from GP histogram density plot. The mixture distribution of the GP histogram density plot, the GP values of P1 and P2 (the maximum of each mixture component), and the mixture weight were calculated from the 2D GP map in MATLAB using the pdf_

normmixture function. Third, HSB images (the GP image normalized by the intensity image), allowing for the visualization of the two domain populations exposing different lipid order (P'1 and P'2), were obtained using a plugging developed in [35].

Statistical analysis

Values are presented as means ± SEM. Statistical significance was tested either with two-sample t-test or one-way ANOVA followed by Tukey's post-hoc test (NS, not significant; * $p < 0.05$; ** $p < 0.01$ and *** $p < 0.001$). Statistical test mentioned above a bar indicates comparison to the control condition (*i.e.* fresh, untreated, healthy RBCs at 20°C), while the significance test above a connecting line indicates a difference inside a group (*e.g.* control, treated, aged, spherocyte or elliptocyte).

Results

Laurdan labelling of living RBCs reveals submicrometric lipid domains

When RBCs were labelled with Laurdan and spread on poly-L-lysine (PLL)-coated coverslips as previously [15, 25-29, 31], well-defined round submicrometric domains (Fig. 1A, arrowheads) and their surrounding membrane were revealed. We then explored

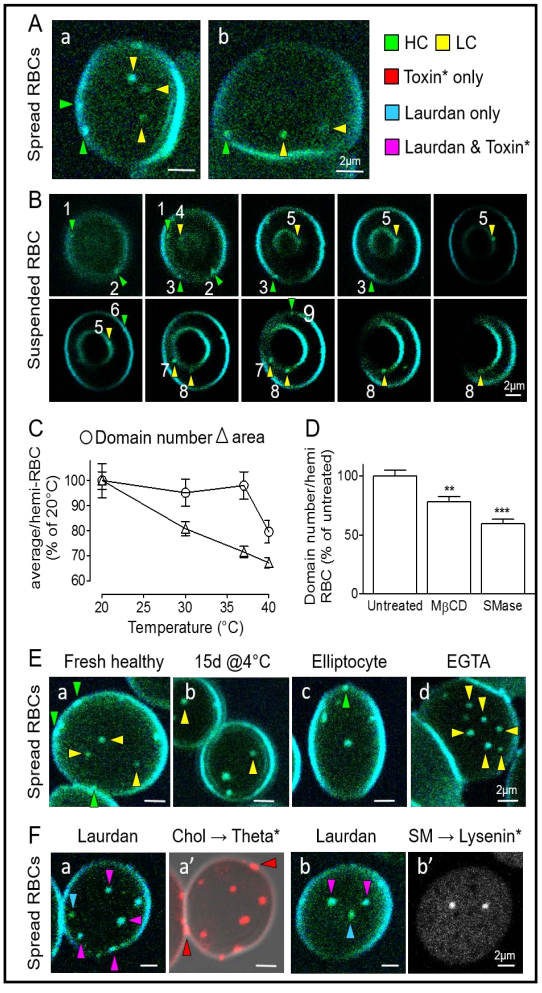

Fig. 1. Labelling of living (*i.e.* non-fixed) RBCs with Laurdan reveals submicrometric domains that largely correspond to those evidenced by the Toxins*. Healthy or elliptocytotic RBCs (elliptocyte, E,c), either fresh (E,a) or maintained at 4°C during 15 days (15d @ 4°C, E,b), were left untreated or treated with EGTA in Ca^{2+}-free medium (EGTA, E,d), labelled with Laurdan alone or Laurdan followed by Toxins* (Theta*, red → Chol or Lysenin*, grey → SM, F), spread onto PLL-coated coverslips (spread) or left in suspension (suspended, B) and observed by vital multiphoton (Laurdan) or multiphoton/confocal (Laurdan+Toxins*) microscopy at 20°C, except at (C). (A) Representative imaging on spread RBCs. Yellow and green arrowheads point respectively to the central area (low curvature, LC) and the edges (high curvature, HC) of the RBC membrane. a and b represent different stages of spreading. (B) Representative imaging on a RBC in suspension. Several stack images were taken for one RBC. Yellow and green arrowheads are associated with a number which refers to the domains observed per image. (C) Quantification of domain number and area (both expressed as percentage of 20°C) in function of temperature. (D) Quantification of domain abundance (average by hemi-RBC expressed as percentage of untreated) upon Chol (MβCD) or SM depletion (SMase). (E) Representative imaging of Laurdan domains upon reshaping. (F) Representative imaging of Laurdan *vs* Toxins. Red, blue and purple arrowheads point respectively to domains revealed by Toxin* only, Laurdan only or both Laurdan and Toxins*. Images are representative from 2–4 independent experiments. Results in C and D are means ± SEM of 211–488 RBCs from 2–4 independent experiments. Statistical significance was tested with one-way ANOVA followed by Tukey's post-hoc test.

whether these domains corresponded to the Chol- and SM/Chol-enriched domains previously evidenced [15, 25] by careful comparison of the behavior of the domains labelled by Laurdan with those revealed by the Toxin* fragments, Theta* and Lysenin*. To confirm our observations we then performed double labelling between Laurdan and the Toxin* fragments.

We first analyzed Laurdan-labelled domain behavior in conditions for which Theta*- and Lysenin*-labelled domains behave similarly, *i.e.* (i) presence in both spread and suspended RBCs [31], (ii) loss upon RBC storage at 4°C [31], (iii) decrease of abundance upon temperature increase from 20 to 37°C [15, 25], and (iv) vanishing upon ~15 % Chol depletion (0.25 mM mβCD, 30 min) and strong decrease upon ~20 % SM depletion (2 mU/ml SMase, 10 min) [15, 25]. Like Toxin*-labelled domains [31], those revealed by Laurdan were present in both spread and suspended RBCs (Fig. 1A, B arrowheads). The multiple stack acquisition on suspended RBCs exposed similar domain abundance than spread RBCs (Fig. 1B *vs* Fig. 1A). In addition, Laurdan-labelled domains were decreased upon storage at 4°C (Fig. 1E,b *vs* a). In contrast to Toxin*-labelled domains, Laurdan-labelled domains exhibited a similar abundance between 20 and 37°C (Fig. 1C). In addition, upon ~15 % Chol depletion by mβCD and ~20 % SM depletion by SMase, Laurdan-labelled domains were only decreased by ~25 % and ~40 % respectively (Fig. 1D). Such differential effect of environmental conditions on Laurdan- and Toxin*-labelled domains could not be due to alteration of Toxin* binding as verified before by preserved I^{125}-Theta* and -Lysenin* binding to RBCs upon treatments and by similar decrease of BODIPY-SM- and Lysenin*-labelled domains upon mβCD treatment. All these results therefore suggested that Laurdan- and Toxin*-labelled domains only partially corresponded.

To gain better insight into this discrepancy, Laurdan-labelled domain behavior was then examined in conditions for which Theta*- and Lysenin*-labelled domains behave differently, *i.e.* (i) different abundance (Theta* >> Lysenin*) [15, 25], (ii) preferential topographic association with the center of low curvature (Low curvature (LC), Lysenin*) *vs* the highly curved edges (High curvature (HC), Theta*) of the RBC membrane [31], (iii) specific vanishing upon increased RBC spreading state (Lysenin*) [15, 25], (iv) specific recruitment in highly curved edges of elliptocytes (Theta*), a model of deformed RBC [31], and (v) specific increased abundance with Ca^{2+} efflux stimulation (Lysenin*) [31]. First, Laurdan-labelled domains (~3 domains/hemi-RBC) exhibited an intermediate abundance between those labelled by Lysenin* and Theta* [15, 25]. Second, they were present both in HC and LC regions, although less abundant than Theta*-labeled domains in HC (compare Fig. 1A with Fig. 1F,a'). Third, Laurdan-labelled domains were moderately affected by increased spreading (Fig. 1A,b *vs* a), as Theta*-labelled domains but in contrast to those labelled by Lysenin* [15, 25]. Fourth, they were revealed in increased curvature areas of the elliptocyte edges (Fig. 1E,c), as Theta*-labelled domains [31]. Fifth, Laurdan-labelled domains were increased in abundance along with Ca^{2+} efflux (Fig. 1E,d), as those revealed by Lysenin* [31]. Altogether, these observations indicated that Laurdan-labelled domains at least partially corresponded to those we previously revealed by Lysenin* and Theta*, although only a part of the Theta*-labelled domain population in HC was labelled by Laurdan.

To further check for this observation, RBCs were double-labelled with Laurdan and Toxins*. As expected, Theta*-labelled domains were partly revealed by Laurdan in HC (Fig. 1F,a,a'; purple *vs* red arrowheads) whereas majority of Theta*- and Lysenin*-labelled domains were revealed by Laurdan in LC (Fig. 1F,a,b; purple arrowheads). Moreover, Laurdan revealed an additional, less abundant, domain population not decorated by Theta* or Lysenin* in LC (blue arrowhead at F,a & b). This additional population labelled by Laurdan could explain the discrepancy of response to environmental conditions (temperature increase and Chol and SM content decrease) as compared to Toxin*-labelled domains. Altogether these data indicated that Laurdan revealed part of the Theta*-labelled domains in HC, the majority of Theta* and Lysenin*-labelled domains in LC and an additional population not decorated by Theta* or Lysenin* in LC.

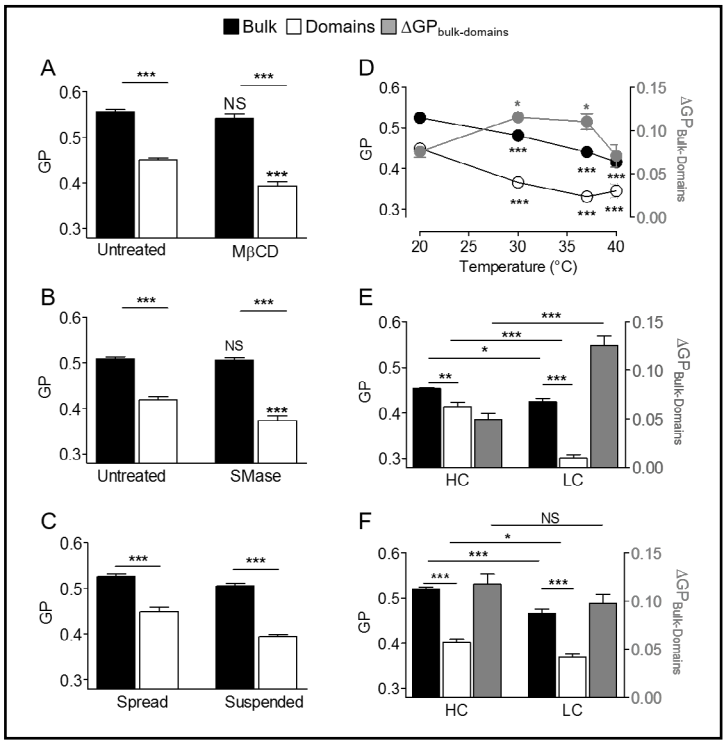

Fig. 2. Lipid domains exhibit a lower order than the bulk membrane. Healthy RBCs, either left untreated or treated with MβCD or SMase (A, B), were labelled with Laurdan, spread onto PLL-coated coverslips or left in suspension (suspended, C) and observed by vital multiphoton microscopy at 20°C (except in D). Bulk (black columns and bullets, left axis) and domain (open columns and bullets, left axis) GP values were then determined and expressed as difference in GP values between bulk and domains ($\Delta GP_{bulk\text{-}domains}$, grey bullets and columns, right axis, D-F) or not (A-C). (A, B) RBCs depleted in Chol (A, MβCD) or SM (B, SMase) and spread; (C) RBCs either spread (spread) or left in suspension (suspended); (D) Spread RBCs analyzed in the 20-40°C temperature range; (E, F) RBCs either spread (E) or suspended (F) and compared for the central area (low curvature, LC) and the edges (high curvature, HC) of the membrane. Results are means ± SEM of 175–352 RBCs from 2–3 independent experiments. Statistical significance was tested with one-way ANOVA followed by Tukey's post-hoc test (open and black columns) or two-sample t-tests (grey columns). A statistical test is denoted above a bar, giving a comparison to the control condition (i.e. fresh, untreated, healthy RBCs at 20°C), while statistical test above a connecting line indicates comparison inside a group.

In RBCs at resting state, submicrometric lipid domains exhibit a lower order than the bulk membrane

We then examined the lipid order of submicrometric lipid domains on spread RBCs at 20°C, while keeping in mind the two differences mentioned above between Laurdan and Toxin* labeling. The GP values extracted from the Laurdan imaging were significantly lower (*i.e.* lower lipid order) for the domains than the bulk (Fig. 2A, untreated). At first glance, this observation was surprising since Laurdan experiments on model membranes show higher lipid order for Chol- and SM-enriched phases [4, 5]. We excluded potential artefacts related to Laurdan physicochemical properties or preferential partitioning. Indeed, the strong photoselection of Laurdan molecules, particularly when located within the more ordered phases [37], was strongly reduced by using a Nomarski prism (see Material and methods Section). We also precluded a preferential partitioning of Laurdan in labelled domains in L_d-phase, as seen for C-Laurdan in GUVs (our unpublished data) or in *N*-palmitoyl-enriched-D-*erythro*-sphingosine-enriched domains [38].

We then asked whether the lower lipid order of domains as compared to the surrounding bulk could be dependent on the RBC membrane composition, RBC spreading, temperature, or membrane curvature. Chol or SM depletion using mβCD or SMase (in the same range of concentrations as above) decreased lipid order of the domains while preserving the bulk (Fig. 2A & B), in agreement with the ordering effect of Chol and SM enrichment on living cells. The lower GP value for the domains than the bulk was further confirmed in suspended RBCs (Fig. 2C) and at temperature ranging from 20 to 40°C with a maximal delta GP bulk-domains ($\Delta GP_{bulk\text{-}domains}$) in the 30-37°C range (Fig. 2D), suggesting physiological relevance. Regarding topography, both lipid domains and bulk membrane exhibited higher order in HC

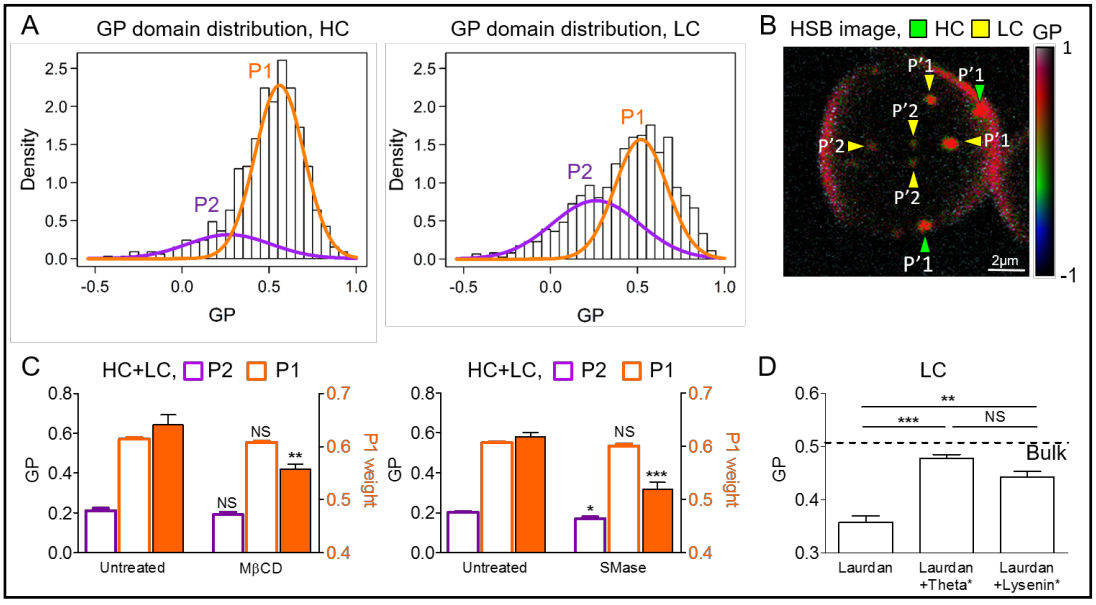

Fig. 3. Three types of lipid domains with distinct lipid order and topography coexist. Fresh healthy RBCs, either left untreated or treated with MβCD or SMase (C), were labelled with Laurdan alone (A-C) or Laurdan followed by Toxins* (D; Theta*→ Chol or Lysenin*→ SM), spread onto PLL-coated coverslips and observed by vital multiphoton (Laurdan alone) or multiphoton/confocal (Laurdan+Toxins*) microscopy at 20°C. (A) GP domain distribution in HC (left panel) and LC (right panel) calculated from one Laurdan image (35 RBCs). Notice one major GP domain population in HC (P1) and two in LC (P1 and P2). (B) Representative HSB imaging of one Laurdan-labelled RBC. Yellow and green arrowheads point respectively to the central area (low curvature, LC) and the edges (high curvature, HC) of the RBC membrane. Notice one GP domain population in HC (P'1) and two in LC (P'1 and P'2). (C) Quantification based on representative data presented at A: GP values of P1 (white columns boxed in orange, left axis) and P2 (white columns boxed in purple) and of the proportion of P1 as compared to P2 (orange columns and left axis) in untreated RBCs or upon Chol or SM depletion. (D) Quantification of GP values for LC domains labelled with Laurdan only (Laurdan) or Laurdan and Toxins* (Laurdan+Theta*, Laurdan+Lysenin*). GP distributions (calculated from 35 RBCs) and the GP image are representative of 6 independent experiments. Results are means ± SEM of 142–352 RBCs from 2–3 independent experiments (C-D). Statistical significance was tested with one-way ANOVA followed by Tukey's post-hoc test or two-sample t-tests (orange columns). Asterisk directly above a bar indicates a mean significantly different from its counterpart in the control condition, while the significance level above a connecting line indicates a difference between two means observed inside a group.

than the center LC areas of the RBC membrane, in spread as well as suspended RBCs (Fig. 2E & F). However, a slight impact of RBC spreading on lipid order was observed, mainly for the domains in HC.

Altogether, these data indicated a differential lipid order between the domains and the bulk, as revealed in the $\Delta GP_{bulk\text{-}domains}$ (Fig. 2D-F, grey symbols and columns and right axes), with lipid domains exhibiting a lower lipid order than the bulk in both spread and suspended RBCs, HC and LC areas and in a large temperature range. Whereas bulk and domain lipid order exposed similar trends in their responses to temperature and membrane curvature, lipid domain order was more dependent than the bulk on PM Chol and SM contents.

Three types of submicrometric lipid domains with distinct order, composition and topography coexist at the RBC plasma membrane

Based on our suggestion for the coexistence of three Laurdan-labelled domain populations (those Chol-enriched in HC, those SM/Chol-coenriched in LC and those not enriched in these lipids in LC) and since lipid domains in HC showed higher order than those in LC, we asked whether the three domain populations could exhibit distinct lipid order. To

this aim, we analyzed the GP distribution of the domains using GP density histograms (Fig. 3A) and GP images (Fig. 3B), both obtained from Laurdan images. In terms of lipid order, while the HC area of the membrane seemed to reveal one domain population (major P1 *vs* P2 contribution in Fig. 3A left; P'1, green arrowheads in Fig. 3B), two populations appeared to coexist in LC (P1 and P2 contribution in Fig. 3A right; P'1 and P'2, yellow arrowheads in Fig. 3B). However, the HC population had a very close GP value to the more ordered population in LC (compare P1 in Fig. 3A left *vs* right, and P'1 in Fig. 3B green *vs* yellow arrowheads). These results suggested the presence of at least two distinct populations in terms of lipid order, a more ordered population associated to both HC and LC (P1 in GP density distribution and P'1 in HSB images) and a less ordered population observed in LC (P2 in GP density distribution and P'2 in HSB images).

We then asked for the identity between these two domain populations, revealed by Laurdan domain GP distribution and imaging, and the three domain populations previously unveiled based on Chol and SM enrichment and topography. We first evaluated the impact of partial Chol or SM depletion on the domain GP distribution, in the conditions for which we previously showed a decrease of the global domain GP value and a higher abrogation of the Chol- and SM-enriched domain populations than on the one not enriched in these lipids. These treatments did not, or only slightly, changed P1 and P2 mean GP values (Fig. 3C) but decreased the contribution of P1 *vs* P2 to the global domain GP distribution (Fig. 3C, orange

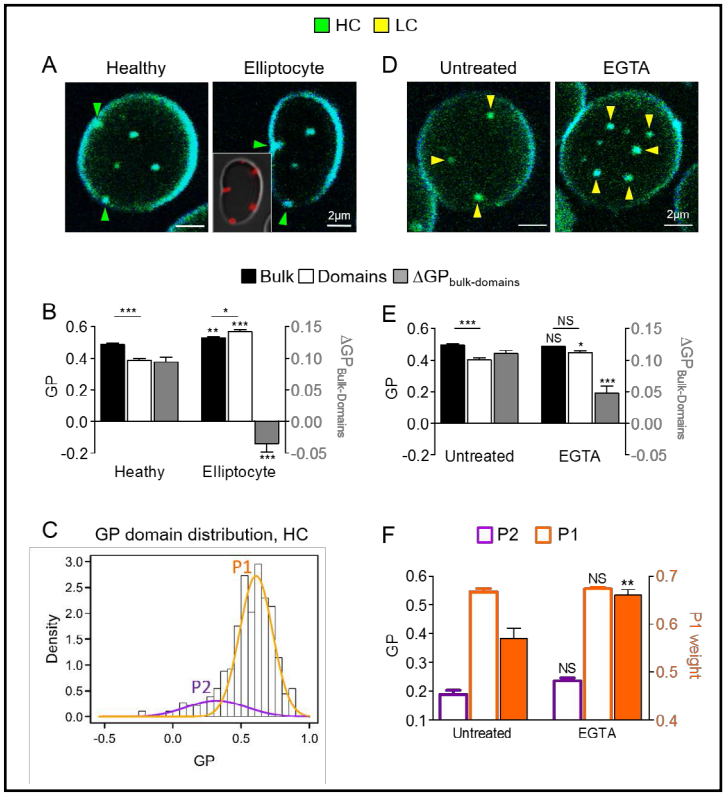

Fig. 4. Lipid domain order increases upon RBC deformation, leading to a decrease of the bulk-domain differential order. Healthy or elliptocytotic (A-C) RBCs were left untreated or treated with EGTA in Ca^{2+}-free medium (EGTA, D-F), labelled with Laurdan alone or Laurdan followed by Theta* (A, inset at right), spread and observed by vital microscopy at 20°C. (A, D) Representative vital imaging. Yellow and green arrowheads point respectively to LC and HC domains. (B, E) Quantification of the GP values of the bulk (black columns, left axis) and domains (open columns, left axis) and difference in bulk and domain GP values ($\Delta GP_{bulk\text{-}domains}$, grey columns, right axis) in HC (B) or LC (E). (C) GP value distribution (expressed as proportion of total values) of HC domains in elliptocytes. One major GP domain population (P1) can be observed. (F) Quantification of the GP values of P1 (white columns boxed in orange, left axis), P2 (white columns boxed in purple, left axis) and of the proportion of P1 as compared to P2 (orange columns, right axis) for RBCs left untreated (untreated) or stimulated for Ca^{2+} efflux (EGTA). Images are representative from 2–3 independent experiments and results are means ± SEM of 340–412 RBCs. Statistical significance was tested with one-way ANOVA followed by Tukey's post-hoc test (black and open columns) or with two-sample t-tests (grey columns). Asterisk directly above a bar indicates a mean significantly different from its counterpart in the control condition, while the significance level above a connecting line indicates a difference between two means observed inside a group.

filled columns and right axes). This suggested that the more ordered P1 population could be mostly influenced by Chol- and SM/Chol-enriched domains while the less ordered P2 population could represent those not enriched in these lipids. This hypothesis was confirmed by analysis of lipid order in RBCs co-labeled with Laurdan and Toxins* which indicated that Laurdan-labelled domains colocalized either with Theta* or Lysenin* exposed a close GP value, significantly higher than those only labelled by Laurdan (Fig. 3D). Furthermore, it should be noticed that the P1 population was considerably more abundant than the P2 one as revealed by P1 weight (Fig. 3C, untreated). Accordingly, the Chol- and SM/Chol-enriched domains were more abundant than those not enriched in these lipids.

All these observations suggested the coexistence at the PM of living RBCs of at least three domain populations in terms of lipid composition, topography and lipid order. The population associated with the edges and enriched in Chol mainly showed a GP value close to the one of the population restricted to the cell center and enriched in both Chol and SM. In contrast, the domain population restricted to the center of the cell but enriched neither in Chol nor SM exhibited a lower GP value than the two other domain populations.

Upon RBC deformation and vesiculation, lipid domain order increases to a similar or higher level than the bulk, leading to a $\Delta GP_{bulk\text{-}domains}$ decrease

We previously exposed the implication of Chol- and SM/Chol-enriched domains in RBC deformation and vesiculation [31]: (i) Chol-enriched domains are recruited in increased curvature areas of the membrane edges upon deformation, (ii) SM/Chol-enriched domains are increased in abundance in low curvature areas, allowing for Ca^{2+} efflux during the following shape and volume restoration, and (iii) both lipid domains are specific sites for membrane vesiculation upon aging [31]. As shown in Fig. 1E, Laurdan-labelled domains were similarly reorganized during these processes. Because the differential lipid order between

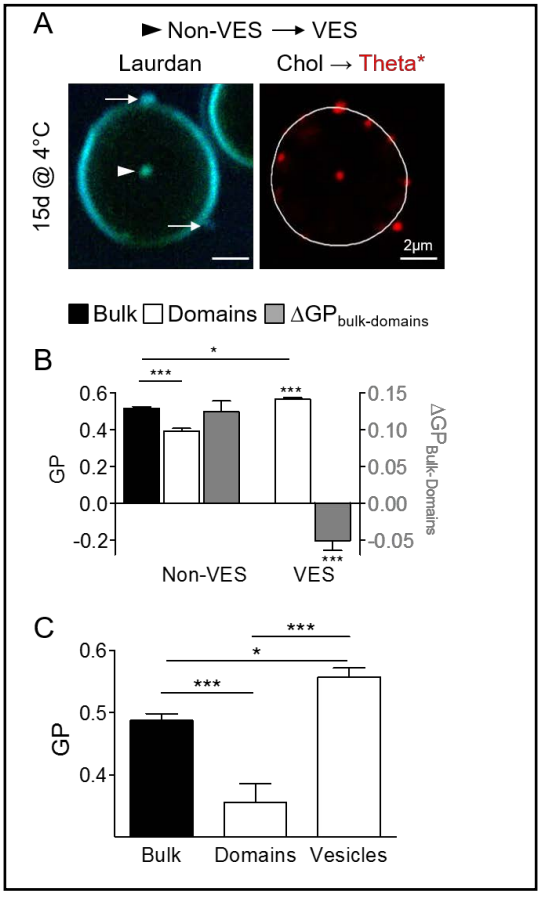

Fig. 5. Lipid domain order increases upon RBC vesiculation, leading to a decrease of the bulk-domain differential order. Healthy RBCs maintained at 4°C during 15 days (15d @ 4°C) were labelled with Laurdan alone (B, C) or Laurdan followed by Theta* (A), spread and observed by vital microscopy at 20°C. (A) Representative vital imaging. White arrowhead and arrows point to non-vesiculating (Non-VES) and vesiculating (VES) Laurdan-labelled Chol-enriched domains in aged RBCs. (B) Quantification of the GP values of the bulk (black columns, left axis) and domains (open columns, left axis) and difference in bulk and domain GP values ($\Delta GP_{bulk\text{-}domains}$, grey columns, right axis) in Non-VES and VES. (C) Quantification of the GP values of the bulk (black column) and domains or vesicles (open columns) in stored RBCs. Images are representative from 2–4 independent experiments and results are means ± SEM of 140–281 RBCs. Statistical significance was tested with one-way ANOVA followed by Tukey's post-hoc test (black and open columns) or with two-sample t-tests (grey columns). Asterisk directly above a bar indicates a mean significantly different from its counterpart in the control condition, while the significance level above a connecting line indicates a difference between two means observed inside a group.

lipid domains and the surrounding membrane is thought to be relevant for cell physiology through its impact on membrane protein sorting [1, 2], we therefore asked whether lipid domain order and differential bulk-domain order ($\Delta GP_{bulk\text{-}domains}$) are modulated during RBC reshaping.

To study lipid domain order in HC upon RBC deformation, we used as previously elliptocytes as a model of affected RBC shape [31]. We first verified by RBC double-labeling with Laurdan and Theta* that Laurdan-labelled domains in HC of elliptocyte membrane corresponded to those enriched in Chol, as previously observed [31] (Fig. 4A, inset at right). We then compared healthy RBCs and elliptocytes for their bulk and domain lipid order in HC (Fig. 4A, green arrowheads). We observed in elliptocytes an increase of the bulk order (Fig. 4B, black columns) along with an even stronger increase of domain lipid order (Fig. 4B, open columns) that reached higher GP value than the one of the bulk, leading to a decreased $\Delta GP_{bulk\text{-}domains}$ (Fig. 4B, grey columns and right axis). The GP density histogram of elliptocyte HC domains revealed only one domain population, as for healthy RBCs (Fig. 4C), suggesting that the global domain order change was not due to the formation of a new domain population with higher order but instead to the order increase of the preexisting one. Altogether, these data indicated that lipid domains in HC can reach a higher order than the bulk.

We then stimulated Ca^{2+} efflux through RBC incubation with a Ca^{2+}-chelating agent (*i.e.* EGTA) in a Ca^{2+}-free medium [31] to induce SM/Chol-enriched domain abundance increase in LC during shape and volume restoration after deformation [24]. This approach, which increased Laurdan-labelled domain abundance in LC (Fig. 4D; 2.5 fold increase) as observed before with Lysenin* or BODIPY-SM [31], slightly increased the lipid order of LC domains while preserving the bulk lipid order, resulting into a decreased $\Delta GP_{bulk\text{-}domains}$ (Fig. 4E). More precisely, we observed an increased proportion of the more ordered P1 population, without significant changes in P1 and P2 lipid order (Fig. 4F). This indicates that the increase of LC domain order by Ca^{2+} efflux stimulation could result from an increased abundance of the more ordered P1 population, as an additional line of evidence for the coexistence of two domain populations in LC and for the correspondence of SM/Chol-enriched domains and P1 populations.

Finally, we took benefit from the possibility to induce lipid domain local vesiculation by RBC storage at 4°C [31] to ask whether lipid domain order is modulated upon their vesiculation. Vesiculating Chol-enriched domains, evidenced by double-labelling with Laurdan and Theta* (Fig. 5A, white arrows), exposed an increased lipid order, that became higher than the bulk and led to a decreased $\Delta GP_{bulk\text{-}domains}$ (Fig. 5B). Similar GP values were obtained for vesicles in aged RBCs labelled with Laurdan only (Fig. 5C). Thus, lipid domains exposed an increased lipid order upon local membrane vesiculation.

Altogether, these data indicated that the lipid order of lipid domains, lower than the one of the bulk in resting RBCs, was increased upon RBC deformation and vesiculation to higher GP values than the bulk, leading to a decreased order difference between the domains and the bulk.

Upon RBC storage at 4°C, bulk lipid order increases, leading to a $\Delta GP_{bulk\text{-}domains}$ increase and domain vesiculation

Upon RBC aging, ATP intracellular content decreases, reducing the frequency of ATP-induced lateral dissociations of the spectrin network, making it more fully connected and stiff [39, 57]. These changes lead to larger compressive forces on the cell membrane and have been hypothesized to be accommodated by increased membrane curvature and vesicle detachment from the membrane [39, 41, 42]. Additionally, theoretical works and experiments on model membranes propose that lipid order disparity between L_o and L_d phases, and the related unfavorable line tension at domain boundary, drives specific domain budding and following fission [43-45]. We therefore asked whether the increased cytoskeleton compression applied to the membrane could contribute, along with changes in lipid order disparity, to the initiation of lipid domain vesiculation in RBCs upon aging, by respectively measuring the GP_{bulk} and the $\Delta GP_{bulk\text{-}domains}$ in RBCs upon storage at 4°C to mimick RBC aging.

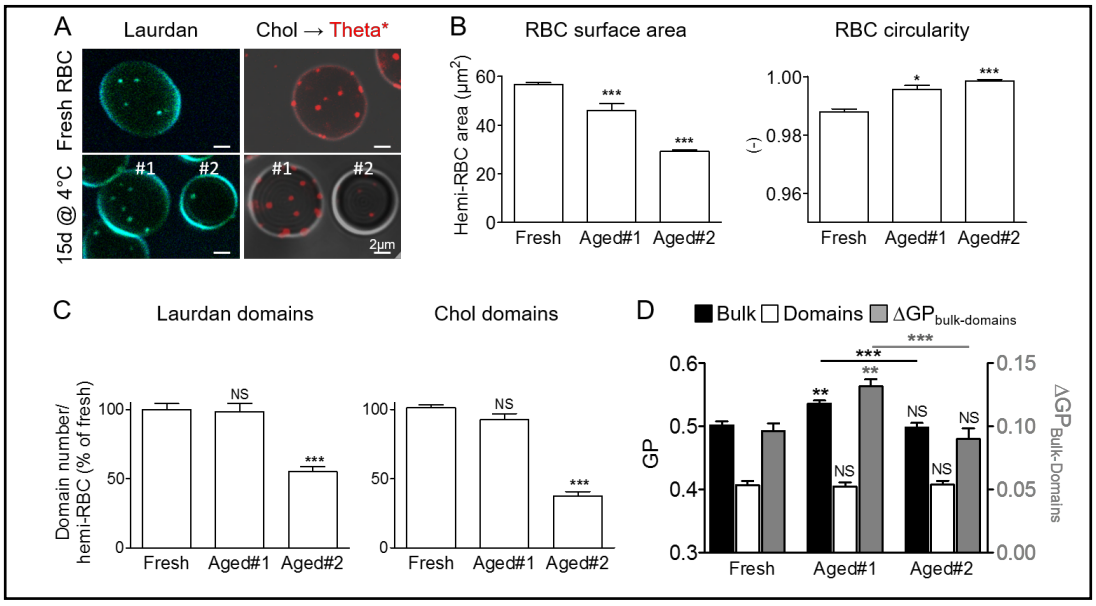

Fig. 6. Bulk membrane order increases upon RBC storage at 4°C, leading to an increase of the bulk-domain differential order and to domain vesiculation. Healthy RBCs, fresh or maintained during 15 days at 4°C (15d @ 4°C), were labelled with Laurdan or Theta* (Chol), spread and observed by vital multiphoton or confocal microscopy at 20°C. #1 and #2 label respectively the first and second stage of aging in terms of RBC surface area and circularity (B) and domain number (C). (A) Representative vital imaging. Images of Theta* labeling were superposed to RBCs in transmission to highlight cell periphery. (B) Quantification of RBC area (µm² by hemi-RBC) and circularity. (C) Quantification of Laurdan- and Theta*-labeled domain abundance (average by hemi-RBC expressed as percentage of fresh RBCs). (D) Quantification of bulk (black columns, left axis) and domain GP values (open columns, left axis) and difference in GP values between bulk and domains ($\Delta GP_{bulk\text{-}domains}$, grey columns, right axis) for fresh RBCs and RBCs at their two stages of aging during the 15 days at 4°C. Images are representative from 2 independent experiments and results are means ± SEM of 37–231 RBCs. Statistical significance was tested with one-way ANOVA followed by Tukey's post-hoc test (black and open columns) or with two-sample t-tests (grey columns). Asterisk directly above a bar indicates a mean significantly different from fresh RBCs, while the significance level above a connecting line indicates a difference between two means observed inside a group.

RBCs upon storage at 4°C were first characterized for their surface area and circularity as well as for their lipid domain abundance (Fig. 6A-C). Two stages of aging were defined: Aged#1, with moderate surface area loss, slight circularity increase and no significant domain loss, and Aged#2, with high membrane loss, high circularity and large domain loss. Aged#1 could therefore correspond to aged RBCs before domain vesiculation, while Aged#2 could represent aged RBCs after major domain vesiculation. Unlike vesiculating domains (see Fig. 5), domain lipid order was not modified upon aging before domain vesiculation (Fig. 6D, open columns and left axis, Aged#1 and Aged#2). In contrast, bulk lipid order was first increased at Aged#1 and thereafter decreased at Aged#2 (Fig. 6D, black columns and left axis). This led to an increased $\Delta GP_{bulk\text{-}domains}$ at Aged#1 stage, *i.e.* prior major domain vesiculation, followed by a decreased $\Delta GP_{bulk\text{-}domains}$ back to its initial value at Aged#2, *i.e.* after major domain vesiculation (Fig. 6D, grey columns and right axis).

Altogether, these data indicated that GP_{bulk} was increased upon aging, leading to an increased $\Delta GP_{bulk\text{-}domains}$ (Aged#1), together with the initiation of domain vesiculation (Aged#2).

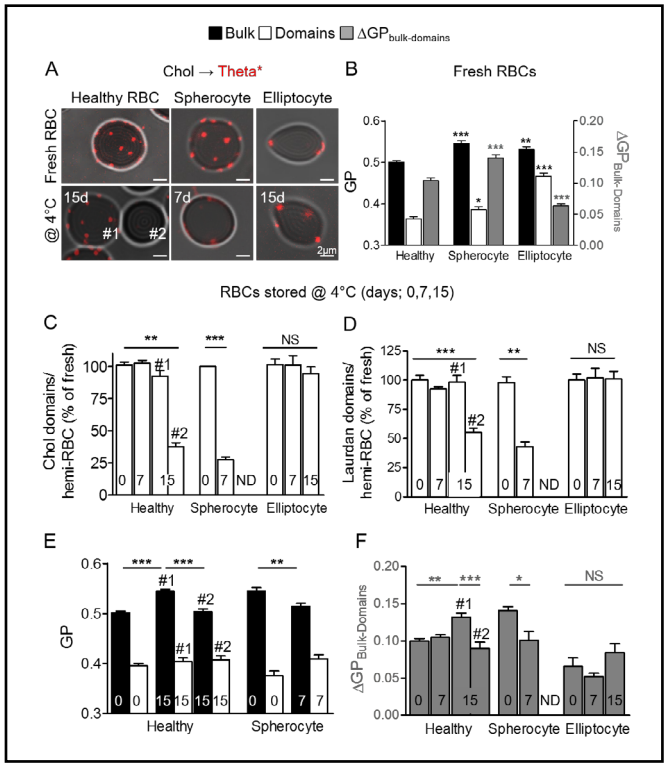

Fig. 7. Spherocytes and elliptocytes respectively exhibit higher and lower bulk-domain differential order than healthy RBCs, resulting into accelerated and reduced domain vesiculation upon aging. Healthy RBCs, spherocytes or elliptocytes, either fresh or maintained for the indicated times at 4°C, were labelled with Laurdan (B, D-F) or Theta* (A, C, Chol), spread and observed by vital multiphoton or confocal microscopy at 20°C. #1 and #2 label respectively the first and second stage of aging, as defined at Fig. 6. (A) Representative vital imaging of Chol-enriched domains upon aging. (B) Quantification of bulk (black columns, left axis) and domain GP values (open columns, left axis) and difference in GP values between bulk and domains ($\Delta GP_{bulk\text{-}domains}$, grey columns, right axis) for fresh healthy RBCs, spherocytes and elliptocytes. (C, D) Quantification of Theta*- (C) and Laurdan-labeled domain number (D; both as average by hemi-RBC expressed as percentage of fresh RBCs). (E, F) Quantification of GP values of the bulk (E; black columns) and domains (E; open columns) and $\Delta GP_{bulk\text{-}domains}$ (F) for healthy RBCs, spherocytes and elliptocytes maintained for the indicated times at 4°C (numbers in columns). Images are representative of 2 independent experiments and results are means ± SEM of 37–231 RBCs. Statistical significance was tested with one-way ANOVA followed by Tukey's post-hoc test. Asterisk directly above a bar indicates a mean significantly different from its counterpart in the control condition while the significance level above a connecting line indicates a difference between two means observed inside a group.

Both $\Delta GP_{bulk\text{-}domains}$ and domain vesiculation are increased in spherocytosis but are decreased in elliptocytosis

We then further investigated the potential link between the increased cytoskeleton compression applied to the membrane (reflected by the GP_{bulk} increase), the increased lipid order disparity (reflected by the $\Delta GP_{bulk\text{-}domains}$ increase) and the initiation of domain vesiculation, using RBCs from a patient with spherocytosis, the most common hereditary RBC membrane disorder caused by defects in proteins that vertically connect the membrane to the cytoskeleton, *i.e.* the ankyrin complexes [46]. Such a protein defect impairs membrane:cytoskeleton cohesion and increases the pressure exerted by the cytoskeleton on the membrane [40], leading to membrane destabilization [39], the release of vesicles and the decrease of the RBC surface area-to-volume ratio and deformability [47], as in RBC aging. In terms of lipid order, the increased membrane pressure should give rise to more compressed and ordered lipids, as observed for RBC aging. As expected, fresh spherocytes exposed a higher increase of lipid order in the bulk (Fig. 7B, black columns and left axis) than in the lipid domains (Fig. 7B, open columns and left axis), leading to an increased $\Delta GP_{bulk\text{-}domains}$ (Fig. 7B, grey columns and right axis). These changes were similar to those observed in healthy Aged#1 RBCs (Fig. 7E; compare fresh and spherocytes with healthy 15d, Aged#1). Upon storage at 4°C for 7 days, spherocytes showed a decrease of both Laurdan-labelled (Fig. 7D) and Chol-enriched domains (Fig. 7A and quantification in Fig. 7C). Such decrease could result from the budding and shedding of Chol-enriched vesicles from the membrane during this time interval, reducing thereby the pressure exerted by the cytoskeleton on the

membrane, as reflected in the decrease of the GP_{bulk} (Fig. 7E) and the $\Delta GP_{bulk\text{-}domains}$ back to their initial values (Fig. 7F). All these changes were similar to those found in healthy Aged#2 RBCs after 15 days of storage (Fig. 7E).

Based on the relation between the increased cytoskeleton compression applied to the membrane, the increased lipid order disparity and the initiation of domain vesiculation observed in both healthy RBC aging and spherocytosis, we then examined lipid order upon lowering of the cytoskeleton pressure, which is expected to produce a lower rate of vesicle shedding. This was achieved by analyzing aging of RBCs from patients with elliptocytosis, a disease due to disruptions of horizontal cytoskeleton interactions, resulting in alteration of the spectrin tetramer self-association and decreased deformability [48]. As already shown at Fig. 4A, fresh elliptocytes exhibited a higher increased lipid order in the domains (Fig. 7B, open columns and left axis) than in the bulk (Fig. 7B, black columns and left axis), leading to a decreased $\Delta GP_{bulk\text{-}domains}$ (Fig. 7B, grey columns and right axis). Moreover, as hypothesized, elliptocytes exhibited no domain loss in the 0-15 days storage (Fig. 7A; quantification in Fig. 7C for Chol-enriched domains and in Fig. 7D for Laurdan-labelled domains) and the lower $\Delta GP_{bulk\text{-}domains}$ in fresh elliptocytes as compared to Aged#1 healthy RBCs or spherocytes was accordingly maintained all along the storage (Fig. 7F).

Altogether, these data indicated that, in comparison to healthy RBCs, fresh spherocytes, which exhibited higher pressure applied by the cytoskeleton on the membrane, exposed higher $\Delta GP_{bulk\text{-}domains}$ together with an accelerated initiation of domain vesiculation upon aging. The opposite was observed for elliptocytes, which exhibited lower pressure applied by the cytoskeleton on the membrane and exposed lower $\Delta GP_{bulk\text{-}domains}$ and reduced domain vesiculation upon aging. This suggests that the cytoskeleton pressure could give the main contribution that controls the $\Delta GP_{bulk\text{-}domains}$ and drives RBC vesiculation.

Discussion

The differential lipid order between lipid rafts and the surrounding bulk membrane is thought to be highly relevant for cell physiology. Based on our recent demonstration of submicrometric domains enriched in Chol or SM/Chol at the living RBC surface [15, 25] and their contribution to RBC deformation and vesiculation upon aging [31], we here asked whether the seminal concept of high ordering of lipid rafts could also be relevant for submicrometric lipid domains. We also explored whether the differential lipid order between submicrometric domains and the surrounding membrane can be modulated by, and/or participate in, cell functions such as RBC reshaping.

Upon Laurdan labeling of the RBC PM, submicrometric domains were revealed, as previously proposed by Sanchez and coll. at the rabbit RBC surface [49]. Thanks to RBC double-labelling with Laurdan and Toxin* fragments, three domain populations were revealed by Laurdan at the resting RBC PM: (i) a part of Theta*-labelled domains in HC; (ii) the vast majority of Theta*- and Lysenin*-labelled domains in LC; and (iii) an additional population in LC, not labelled by the Toxins*. By analysis of the GP distribution on GP histogram density plots and GP images, two very distinct populations were evidenced in terms of lipid order: (i) one more ordered, more abundant and present in both HC and LC, and (ii) another less ordered, less abundant and associated to LC. Based on membrane Chol and SM content decrease using pharmacological agents and co-labelling of Laurdan with the Toxins*, we suggested that the first population corresponded to Chol-enriched domains in HC and to SM/Chol coenriched domains in LC, while the second one corresponded to domains not enriched in these lipids and labeled by Laurdan alone in LC.

Regarding GP values of lipid domains *vs* the bulk membrane, the range we showed in living resting RBCs was smaller than the one observed in sterol-containing biomimetic GUVs [4, 5], but close to that observed on the more natural GPMVs [7]. This was not surprising since biological membranes likely maintain rather small order differences, as this configuration could allow cells to modulate them with relatively little energy input. More amazing was

that the different lipid domain populations in fresh healthy RBCs at resting state exhibited lower order than the bulk, whatever the temperature, RBC spreading state and membrane curvature. Although in agreement with the major coverage of the membrane by an ordered phase in rabbit RBCs [49], apical membranes of polarized epithelial cells [50], CHO cells [49] and HeLa cells [1], our observation did not fit with the higher lipid order of rafts as compared to the surrounding bulk lipids. Several non-exclusive explanations can be provided to explain the lower GP values of Laurdan-labelled domains than the bulk. The first one relates to the higher curvature that the domains could adopt [51], whereby a higher positive curvature would allow for more water penetration, resulting in a red-shift of the laurdan emission spectra and a decrease of its GP [52]. Second, a reduced GP in the domains as compared to the bulk could result from a partial loss of membrane asymmetry in those spots. This hypothesis is unlikely since fresh RBCs can be not highlighted with Annexin V, a fluorescent probe for outer leaflet phosphatidylserine, indicating preservation of lipid asymmetry in fresh RBCs at resting state (unpublished data). Third, a differential enrichment in membrane proteins between the bulk and the domains could contribute to regulate their distinct lipid order. Indeed, transmembrane proteins have been shown to restrict lipid lateral mobility in the RBC membrane [53]. This is also suggested by our results since lipid domain and bulk lipid order increased during their local vesiculation, yet RBC vesicles are highly enriched in proteins [54] and RBC bulk lipid order decreases after vesiculation (Aged#2). Fourth, the calcium and ATP intracellular contents and exchanges could also contribute to regulate lipid domain order. We indeed observed an increased lipid order of lipid domains upon stimulation of calcium efflux through RBC incubation with a calcium-chelating agent in a calcium-free medium. Accordingly, using rabbit RBCs incubated in a calcium- and glucose-free medium, Sanchez and coll. evidenced by combined Laurdan GP imaging and scanning FCS domains that exhibit tighter packing than the fluid phase [49].

Although lipid domains all exhibited a lower GP value than the bulk at RBC resting state, it should be noticed that only a part of the Theta*-labelled domain population in high curvature areas was labelled by Laurdan. We can therefore not exclude the possibility that the Chol-enriched domain population that was not revealed by Laurdan exhibits a higher order than the bulk. Accordingly, high spatial resolution atomic force microscopy of the RBC membrane allowed us to reveal lipid domains correlated with both local minima and maxima areas in the Young's modulus maps [33]. This suggests that the RBC membrane is composed of lipid domains exhibiting differential local mechanical properties, which could depend on the specific lipid domain composition and on their differential association to membrane and cytoskeletal proteins.

Since the differential bulk-domain lipid order was systematically modulated in RBC aging, in spherocytosis and in elliptocytosis, the cytoskeleton density and its membrane anchorage should play a key role in controlling bulk membrane lipid order and the differential lipid order between the domains and the bulk. We propose that bulk membrane, but not (or in a lesser extent) lipid domains, exhibits high connectivity to the cytoskeleton, in turn causing higher lipid order through the spectrin filaments and/or the membrane:cytoskeleton anchorage complexes. Three lines of evidence support this hypothesis. First, upon RBC labeling of CD47 to identify ankyrin-based complexes in healthy RBCs, we have previously shown that antibody-induced CD47 patches and lipid domains (revealed upon insertion of BODIPY-lipids) are not colocalized but are in close proximity [28], suggesting the preferential membrane:cytoskeleton interaction outside of the domains. Second, we observed an increase of the bulk lipid order in spherocytosis. If the GP value serves as a sensor for the compressive pressure applied by the cytoskeleton on the membrane, higher bulk order corresponds to higher compression due to the cytoskeleton. This is exactly what we observed in RBCs of the patient suffering from spherocytosis included in this study, which exhibit an increased spectrin network density (unpublished; confocal and transmission electron microscopy). It remains to be determined how interactions with anchorage complexes are also affected in these spherocytotic RBCs, but theoretical studies show that the loss of the spectrin:membrane anchorage stiffens the cytoskeleton [40, 55]. These spherocytotic RBCs also have a higher

content of intracellular calcium, known to increase the connectivity of the RBC cytoskeleton [56], and resulting in higher membrane compression [57]. Third, lipid order of the bulk membrane was similarly increased in aged RBCs, which exhibit higher calcium content and reduced ATP level [58]. Since both features are known to give rise to more fully connected spectrin network and higher compression, this represents an additional line of evidence for the increased lipid order of the bulk membrane due to higher connectivity to the cytoskeleton.

The increased lipid order of the bulk membrane observed upon RBC aging and in spherocytosis could result in membrane vesiculation, allowing for reduction of the membrane compression. Indeed, it has been hypothesized several years ago that upon RBC aging the larger compressive forces on the cell membrane due to cytoskeleton stiffness and density increase could be accommodated by increased membrane curvature and vesicle detachment from the membrane [39, 41]. Accordingly, based on a two-component coarse-grained molecular dynamics RBC membrane model, Li and Lykotrafitis have revealed that lateral compression generates large vesicles with heterogeneous composition, similar in size to the cytoskeleton corral [59]. The lower vesiculation we observed here in elliptocytosis is also in agreement with the role of the cytoskeleton, since a lower compression is expected to occur in elliptocytotic RBCs. Besides the cytoskeleton pressure, we suggest that the biophysical properties of the lipid domain that will become a vesicle, *i.e.* differential order between bulk and domains, also represent a key feature in driving the budding vesicle. This is supported by the following lines of evidence (i) vesicles generated upon RBC storage are rich in the lipid raft marker stomatin [60]; (ii) loss of Chol- and SM-enriched domains by vesiculation is evident after 15 days of RBC storage [31]; (iii) healthy RBCs showed a $\Delta GP_{bulk-domains}$ increase upon aging (Aged#1), resulting from bulk order increase and preceding domain vesiculation (Aged#2); (iv) fresh spherocytes exposed an increased $\Delta GP_{bulk-domains}$, along with accelerated domain vesiculation upon aging, as compared to healthy RBCs; (v) fresh and aged elliptocytes exposed a lower $\Delta GP_{bulk-domains}$, along with a reduced domain vesiculation upon aging, as compared to healthy RBCs; and (vi) both aged healthy RBCs and spherocytes did not vesiculate anymore when $\Delta GP_{bulk-domains}$ decreased back to its initial value in fresh healthy RBCs. We propose that this increase in the bulk-domain differential lipid order could increase line tension at domain boundary, thereby acting as triggering event for domain vesiculation. Indeed, the line tension at L_o/L_d boundary increases quadratically with thickness difference between the phases [45, 61, 62]. Whether L_o/L_d lipid order difference could also reflect the line tension is unknown, yet is supported by C-Laurdan experiments on GPMVs exposing a strong linear correlation between $\Delta GP_{Lo/Ld}$ and T_{mix} [63], the line tension being proportional to T_{mix} [45] (however not in a simple way for complex membrane systems [64, 65]). Additionally, theoretical works suggest that the reduction of the domain-bulk interface length, hence the line tension energy associated at the boundaries between coexisting fluid (L_o/L_d) domains, is the driving force for domain budding and fission [66]. If so, the compressive force and the line tension can act together to complete the bud growth and detachment in a "synergistic" model where the cytoskeleton pressure on the membrane plays a major role and is coupled to the lipid order properties of the nascent budding vesicle: cytoskeleton compression causes the initial bud to form from a lipid domain exhibiting a differential local curvature, lipid composition and lipid order compared to the surrounding membrane. This model is in agreement with theoretical studies that proposed the forces applied to the membrane by the cytoskeleton combined with lipid composition segregation can drive vesiculation [39]. Besides vesiculation, RBC endovesiculation seems also be governed by the dynamic coupling between membrane and the cytoskeleton [67, 68].

Upon RBC reshaping, lipid order associated to the Chol-enriched domains increased to higher level than the bulk, as revealed in elliptocytotic RBCs. Since lipids are unlikely to contribute alone to membrane curvature [69], changes in lipid order could reflect lipid interaction with membrane bending proteins [70] or cytoskeleton proteins [71]. In favor of the latter hypothesis, the weaker cytoskeleton network due to impairment of horizontal links in elliptocytosis exerts a weaker compression on the membrane. The domains may therefore be less curved and present higher order as compared to healthy RBCs. We still need

to explore whether changes of lipid domain order can influence and/or can be influenced by protein sorting.

Overall, this study demonstrates that the lipid order of submicrometric domains differs from the one of the bulk and can be modulated by, and is involved in, physiological processes such as RBC reshaping. Furthermore, we propose that the differential lipid order between the domains and the bulk can be tuned by cells, through cytoskeleton compression applied to the membrane to use the line tension energy at domain boundary as a control mechanism of lipid domain participation in vesiculation. Besides lipid order, it would be appealing to evaluate other biophysical properties that are known to participate to the line tension energy (*e.g.* domain bending rigidity, intrinsic curvature or thickness) and alternative control mechanisms than membrane:cytoskeleton anchorage (*e.g.* membrane bending proteins and charge-mediated sequestration). Altogether, this study brings new concepts regarding the complexity and tunability of membrane lipid heterogeneities and their participation to cellular functions.

Acknowledgements

We thank Drs. A. Miyawaki, M. Abe and T. Kobayashi (Riken Brain Science Institute, Saitama, Japan & University of Strasbourg, France) as well as H. Mizuno (KU Leuven, Belgium) for generously supplying the Dronpa-NT-Lysenin and Dronpa-theta-D4 plasmids. We also thank V. Mohymont (UCL) for technical support and J. Lorent for reviewing the article. This work was supported by grants from UCL (FSR and Actions de Recherche Concertées, ARC), F.R.S-FNRS and the Salus Sanguinis foundation. N.S.G. is the incumbent of the Lee and William Abramowitz Professorial Chair of Biophysics.

Disclosure Statement

The authors declare to have no competing interests.

References

1 Owen DM, Williamson DJ, Magenau A, Gaus K: Sub-resolution lipid domains exist in the plasma membrane and regulate protein diffusion and distribution. Nature Comm 2012;3:1256.
2 Stone MB, Shelby SA, Núñez MF, Wisser K, Veatch SL: Protein sorting by lipid phase-like domains supports emergent signaling function in B lymphocyte plasma membranes. eLife 2017;6:e19891.
3 Lorent JH, Diaz-Rohrer B, Lin X, Spring K, Gorfe AA, Levental KR: Structural determinants and functional consequences of protein affinity for membrane rafts. Nature Commun 2017;8:1219.
4 Dietrich C, Bagatolli LA, Volovyk ZN, Thompson NL, Levi M, Jacobson K, Gratton E: Lipid Rafts Reconstituted in Model Membranes. Biophys J 2001;80:1417-1428.
5 Jacobson K, Mouritsen OG, Anderson RG: Lipid rafts: at a crossroad between cell biology and physics. Nature Cell Biol 2007;9:7-14.
6 Baumgart T, Hammond AT, Sengupta P, Hess ST, Holowka DA, Baird BA, Webb WW: Large-scale fluid/fluid phase separation of proteins and lipids in giant plasma membrane vesicles. Proc Natl Acad Sci USA 2007;104:3165-3170.
7 Sezgin E, Gutmann T, Buhl T, Dirkx R, Grzybek M, Coskun Ü, Solimena M, Simons K, Levental I, Schwille P: Adaptive lipid packing and bioactivity in membrane domains. PloS One 2015;10:e0123930.
8 Owen DM, Oddos S, Kumar S, Davis DM, Neil MAA, French PMW, Dustin ML, Magee AI, Cebecauer M: High plasma membrane lipid order imaged at the immunological synapse periphery in live T cells. Mol Membr Biol 2010;27:178-189.

9 Rentero C, Zech T, Quinn CM, Engelhardt K, Williamson D, Grewal T, Jessup W, Harder T, Gaus K: Functional Implications of Plasma Membrane Condensation for T Cell Activation. PLoS One 2008;3:e2262.
10 Gaus K, Chklovskaia E, Fazekas de St Groth B, Jessup W, Harder T: Condensation of the plasma membrane at the site of T lymphocyte activation. J Cell Biol 2005;171:121-131.
11 Aresta-Branco F, Cordeiro AM, Marinho HS, Cyrne L, Antunes F, de Almeida RFM: Gel Domains in the Plasma Membrane of Saccharomyces cerevisiae. J Biol Chem 2011;286:5043-5054.
12 Grossmann G, Opekarová M, Malinsky J, Weig-Meckl I, Tanner W: Membrane potential governs lateral segregation of plasma membrane proteins and lipids in yeast. EMBO J 2007;26:1-8.
13 Frisz JF, Lou K, Klitzing HA, Hanafin WP, Lizunov V, Wilson RL, Carpenter KJ, Kim R, Hutcheon ID, Zimmerberg J, Weber PK, Kraft ML: Direct chemical evidence for sphingolipid domains in the plasma membranes of fibroblasts. Proc Natl Acad Sci USA 2013;110:E613-622.
14 Frisz JF, Klitzing HA, Lou K, Hutcheon ID, Weber PK, Zimmerberg J, Kraft ML: Sphingolipid domains in the plasma membranes of fibroblasts are not enriched with cholesterol. J Biol Chem 2013;288:16855-16861.
15 Carquin M, Conrard L, Pollet H, Van Der Smissen P, Cominelli A, Veiga-da-Cunha M, Courtoy PJ, Tyteca D: Cholesterol segregates into submicrometric domains at the living erythrocyte membrane: evidence and regulation. Cell Mol Life Sci 2015;72:4633-4651.
16 van den Bogaart G, Meyenberg K, Risselada HJ, Amin H, Willig KI, Hubrich BE, Dier M, Hell SW, Grubmüller H, Diederichsen U, Jahn R: Membrane protein sequestering by ionic protein–lipid interactions. Nature 2011;479:552-555.
17 Gomez J, Sagues F, Reigada R: Effect of integral proteins in the phase stability of a lipid bilayer: application to raft formation in cell membranes. J Chem Phys 2010;132:135104.
18 Raghupathy R, Anilkumar AA, Polley A, Singh PP, Yadav M, Johnson C, Suryawanshi S, Saikam V, Sawant SD, Panda A, Guo Z, Vishwakarma RA, Rao M, Mayor S: Transbilayer Lipid Interactions Mediate Nanoclustering of Lipid-Anchored Proteins. Cell 2015;161:581-594.
19 Kusumi A, Suzuki KGN, Kasai RS, Ritchie K, Fujiwara TK: Hierarchical mesoscale domain organization of the plasma membrane. Trends Biochem Sci 2011;36:604-615.
20 Kraft ML: Plasma membrane organization and function: moving past lipid rafts. Mol Biol Cell 2013;24:2765-2768.
21 Sevcsik E, Schütz GJ: With or without rafts? Alternative views on cell membranes. Bioessays 2016;38:129-139.
22 Bernardino de la Serna J, Schütz GJ, Eggeling C, Cebecauer M: There Is No Simple Model of the Plasma Membrane Organization. Front Cell Dev Biol 2016;4:106.
23 Gomez-Llobregat J, Buceta J, Reigada R: Interplay of cytoskeletal activity and lipid phase stability in dynamic protein recruitment and clustering. Sci Rep 2013;3:2608.
24 Leonard C, Alsteens D, Dumitru A, Mingeot-Leclercq M, Tyteca D: Lipid domains and membrane (re) shaping : from biophysics to biology; in: Ruysschaert J, Epand R (eds): The Biophysics of Cell Membranes. Biological Consequences. Springer Series in Biophysics, Springer Singapore, 2017, pp. 121-175.
25 Carquin M, Pollet H, Veiga-da-Cunha M, Cominelli A, Van Der Smissen P, N'Kuli F, Emonard H, Henriet P, Mizuno H, Courtoy PJ, Tyteca D: Endogenous sphingomyelin segregates into submicrometric domains in the living erythrocyte membrane. J Lipid Res 2014;55:1331-1342.
26 D'auria L, Van Der Smissen P, Bruyneel F, Courtoy PJ, Tyteca D: Segregation of Fluorescent Membrane Lipids into Distinct Micrometric Domains: Evidence for Phase Compartmentation of Natural Lipids? PLoS One 2011;6:e17021.
27 D'Auria L, Deleu M, Dufour S, Mingeot-Leclercq MP, Tyteca D: Surfactins modulate the lateral organization of fluorescent membrane polar lipids: A new tool to study drug:membrane interaction and assessment of the role of cholesterol and drug acyl chain length. Biochim Biophys Acta (Biomembranes) 2013;1828:2064-2073.
28 D'Auria L, Fenaux M, Aleksandrowicz P, Van Der Smissen P, Chantrain C, Vermylen C, Vikkula M, Courtoy PJ, Tyteca D: Micrometric segregation of fluorescent membrane lipids: relevance for endogenous lipids and biogenesis in erythrocytes. J Lipid Res 2013;54:1066-1076.
29 Tyteca D, D'Auria L, Der Smissen PV, Medts T, Carpentier S, Monbaliu JC, de Diesbach P, Courtoy PJ: Three unrelated sphingomyelin analogs spontaneously cluster into plasma membrane micrometric domains. Biochim Biophys Acta (Biomembranes) 2010;1798:909-927.

30 Carquin M, D'Auria L, Pollet H, Bongarzone ER, Tyteca D: Recent progress on lipid lateral heterogeneity in plasma membranes: From rafts to submicrometric domains. Prog Lipid Res 2016;62:1-24.
31 Leonard C, Conrard L, Guthmann M, Pollet H, Carquin M, Vermylen C, Gailly P, Van Der Smissen P, Mingeot-Leclercq MP, Tyteca D: Contribution of plasma membrane lipid domains to red blood cell (re)shaping. Sci Rep 2017;7:4264.
32 Mohandas N, Gallagher PG: Red cell membrane: past, present, and future. Blood 2008;112:3939-3948.
33 Dumitru AC, Poncin M, Conrard L, Dufrêne Y, Tyteca D, Alsteens D: Nanoscale membrane architecture of healthy and pathological red blood cells. Nanoscale Horiz 2018;3:293-304.
34 Kaiser H-J, Lingwood D, Levental I, Sampaio JL, Kalvodova L, Rajendran L, Simons K: Order of lipid phases in model and plasma membranes. Proc Natl Acad Sci USA 2009;106:16645-16650.
35 Owen DM, Rentero C, Magenau A, Abu-Siniyeh A, Gaus K: Quantitative imaging of membrane lipid order in cells and organisms. Nature Protoc 2011;7:24-35.
36 Parasassi T, Gratton E, Yu WM, Wilson P, Levi M: Two-photon fluorescence microscopy of laurdan generalized polarization domains in model and natural membranes. Biophys J 1997;72:2413-2429.
37 Fidorra M, Heimburg T, Bagatolli LA: Direct visualization of the lateral structure of porcine brain cerebrosides/POPC mixtures in presence and absence of cholesterol. Biophys J 2009;97:142-154.
38 Pinto SN, Fernandes F, Fedorov A, Futerman AH, Silva LC, Prieto M: A combined fluorescence spectroscopy, confocal and 2-photon microscopy approach to re-evaluate the properties of sphingolipid domains. Biochim Biophys Acta (Biomembranes) 2013;1828:2099-2110.
39 Sens P, Gov N: Force Balance and Membrane Shedding at the Red-Blood-Cell Surface. Phys Rev Lett 2007;98:018102.
40 Gov NS: Less is more: removing membrane attachments stiffens the RBC cytoskeleton. New J Phys 2007;9:429.
41 Fricke K, Sackmann E: Variation of frequency spectrum of the erythrocyte flickering caused by aging, osmolarity, temperature and pathological changes. Biochim Biophys Acta (Molecular Cell Research) 1984;803:145-152.
42 Gov N, Cluitmans J, Sens P, Bosman GJCGM: Cytoskeletal control of red blood cell shape: Theory and practice of vesicle formation. Adv Planar Lipid Bilayers Liposomes 2009;10:95-119.
43 Jülicher, Lipowsky: Domain-induced budding of vesicles. Phys Rev Lett 1993;70:2964-2967.
44 Baumgart T, Hess ST, Webb WW: Imaging coexisting fluid domains in biomembrane models coupling curvature and line tension. Nature 2003;425:821-824.
45 García-Sáez AJ, Chiantia S, Schwille P: Effect of line tension on the lateral organization of lipid membranes. J Biol Chem 2007;282:33537-33544.
46 Eber S, Lux SE: Hereditary spherocytosis--defects in proteins that connect the membrane skeleton to the lipid bilayer. Semin Hematol 2004;41:118-141.
47 Perrotta S, Gallagher PG, Mohandas N: Hereditary spherocytosis. Lancet 2008;372:1411-1426.
48 Diez-Silva M, Dao M, Han J, Lim CT, Suresh S: Shape and Biomechanical Characteristics of Human Red Blood Cells in Health and Disease. MRS Bull 2010;35:382-388.
49 Sanchez SA, Tricerri MA, Gratton E: Laurdan generalized polarization fluctuations measures membrane packing micro-heterogeneity *in vivo*. Proc Natl Acad Sci USA 2012;109:7314-7319.
50 Meder D, Moreno MJ, Verkade P, Vaz WLC, Simons K: Phase coexistence and connectivity in the apical membrane of polarized epithelial cells. Proc Natl Acad Sci USA 2006;103:329-334.
51 Ursell TS, Klug WS, Phillips R: Morphology and interaction between lipid domains. Proc Natl Acad Sci USA 2009;106:13301-13306.
52 Parasassi T, Di Stefano M, Loiero M, Ravagnan G, Gratton E: Cholesterol modifies water concentration and dynamics in phospholipid bilayers: a fluorescence study using Laurdan probe. Biophys J 1994;66:763-768.
53 Golan DE, Alecio MR, Veatch WR, Rando RR: Lateral mobility of phospholipid and cholesterol in the human erythrocyte membrane: effects of protein-lipid interactions. Biochemistry 1984;23:332-339.
54 D'Alessandro A, Liumbruno G, Grazzini G, Zolla L: Red blood cell storage: the story so far. Blood Transfus 2010;8:82-88.
55 Lai L, Xu X, Lim Chwee T, Cao J: Stiffening of Red Blood Cells Induced by Cytoskeleton Disorders: A Joint Theory-Experiment Study. Biophys J 2015;109:2287-2294.
56 Liu F, Mizukami H, Sarnaik S, Ostafin A: Calcium-dependent human erythrocyte cytoskeleton stability analysis through atomic force microscopy. J Struct Biol 2005;150:200-210.

57 Gov NS, Safran SA: Red blood cell membrane fluctuations and shape controlled by ATP-induced cytoskeletal defects. Biophys J 2005;88:1859-1874.
58 Rabini RA, Petruzzi E, Staffolani R, Tesei M, Fumelli P, Pazzagli M, Mazzanti L: Diabetes mellitus and subjects' ageing: a study on the ATP content and ATP-related enzyme activities in human erythrocytes. Eur J Clin Invest 1997;27:327-332.
59 Li H, Lykotrafitis G: Vesiculation of healthy and defective red blood cells. Phys Rev E Stat Nonlin Soft Matter Phys 2015;92:015715.
60 Salzer U, Zhu R, Luten M, Isobe H, Pastushenko V, Perkmann T, Hinterdorfer P, Bosman GJ: Vesicles generated during storage of red cells are rich in the lipid raft marker stomatin. Transfusion 2008;48:451-462.
61 Akimov SA, Kuzmin PI, Zimmerberg J, Cohen FS: Lateral tension increases the line tension between two domains in a lipid bilayer membrane. Phys Rev E Stat Nonlin Soft Matter Phys2007;75:011919.
62 Kuzmin PI, Akimov SA, Chizmadzhev YA, Zimmerberg J, Cohen FS: Line Tension and Interaction Energies of Membrane Rafts Calculated from Lipid Splay and Tilt. Biophys J 2005;88:1120-1133.
63 Levental I, Veatch SL: The Continuing Mystery of Lipid Rafts. J Mol Biol 2016;428:4749-4764.
64 Heberle FA, Petruzielo RS, Pan J, Drazba P, Kučerka N, Standaert RF, Feigenson GW, Katsaras J: Bilayer thickness mismatch controls domain size in model membranes. J Am Chem Soc 2013;135:6853-6859.
65 Bleecker JV, Cox PA, Foster RN, Litz JP, Blosser MC, Castner DG, Keller SL: Thickness Mismatch of Coexisting Liquid Phases in Noncanonical Lipid Bilayers. J Phys Chem B 2016;120:2761-2770.
66 Lipowsky R: Budding of membranes induced by intramembrane domains. Journal de Physique II 1992;2:1825-1840.
67 Oberwagner W, Sauer T, Hermann A, Prohaska R, Mullner EW, Salzer U: Drug-induced endovesiculation of erythrocytes is modulated by the dynamics in the cytoskeleton/membrane interaction. Blood Cells Mol Dis 2017;64:15-22.
68 Gov N, Mullner EW, Salzer U: Cytoskeletal connectivity may guide erythrocyte membrane ex- and invagination - A discussion point how biophysical principles might be exploited by a parasite invading erythrocytes. Blood Cells Mol Dis 2017;65:78-80.
69 Zimmerberg J, Kozlov MM: How proteins produce cellular membrane curvature. Nat Rev Mol Cell Biol 2006;7:9-19.
70 Zhao H, Michelot A, Koskela EV, Tkach V, Stamou D, Drubin DG, Lappalainen P: Membrane-Sculpting BAR Domains Generate Stable Lipid Microdomains. Cell Reports 2013;4:1213-1223.
71 Arumugam S, Bassereau P: Membrane nanodomains: contribution of curvature and interaction with proteins and cytoskeleton. Essays Biochem 2015;57:109-119.